Multilayer Analysis: Quantitative Scanning Acoustic Microscopy for Tissue Characterization at a Microscopic Scale

Kay Raum, *Member, IEEE*, Klaus V. Jenderka, *Member, IEEE*, Albrecht Klemenz, and Jörg Brandt

Abstract—An in vitro acoustic microscopy method for the quantitative characterization of biological hard tissues at a microscopic scale is described. At a frequency of 900 MHz, the acoustic impedance is measured as a tissue parameter, which is closely related to its elastomechanical properties. Contrast influences caused by defocus, edges, and surface inclinations, respectively, are either compensated or excluded from the measurement by a special data acquisition and analysis concept. A raster grid was used to validate the capabilities and limitations of the method, and results obtained from human cortical bone are shown. The comparison of different evaluation methods demonstrate the significance of a sophisticated analysis under consideration of topographical and system parameters. Cortical bone impedance maps showed a strong dependence on the anatomical structures, and the mean values were found to be in the range from 3.5 to 6.5 Mrayl within one single osteon.

I. INTRODUCTION

BIOLOGICAL tissue is usually composed of different constructive units of varying size and properties, which results in heterogeneous acoustic properties. For the in vivo characterization of the structural and mechanical properties of bone, ultrasound methods with wavelengths and beam dimensions much larger than the dimensions of the building units usually are applied. The measured bulk parameters are influenced by scattering, interference, and diffraction of the waves during the propagation through the tissue. These parameters are dependent on the composition, structure, and mechanical properties. Extensive work done on low frequency bone characterization aimed to quantify the individual influences [1]–[9], and empirical correlations between functional mechanical parameters (e.g., mineralization, bone density, porosity) and acoustical quantities (e.g., reflection coefficient, speed of sound, broadband attenuation) have been found in different frequency ranges [10]–[17]. However, a physical model that could explain the individual influences of structural and constitutional properties of the bone compound on the sound propagation properties does not yet exist [18].

K. Raum, K.-V. Jenderka, and A. Klemenz are with the Institute of Medical Physics and Biophysics, Martin-Luther-University of Halle Wittenberg, 06097 Halle/Saale, Germany (e-mail: kay.raum@medizin.uni-halle.de).

J. Brandt is with the Orthopedical Clinic, Martin-Luther-University of Halle-Wittenberg, 06097 Halle/Saale, Germany.

Scanning acoustic microscopy (SAM) can be used for in vitro investigations in which the dimensions of wavelength and lateral resolution are comparable to the microscopic constructive units. Since its introduction by Lemons and Quate [19], SAM has become an attractive tool for material characterization as well as for the investigation of biological tissues. One of the prominent features for material characterization of solids is the measurement of surface wave velocities from oscillations in the so-called $V(z)$-curve. This arises from the generation of leaky surface waves in high velocity materials and its interference with reflected waves, while the acoustic lens is moved successively toward the surface of the sample. The dependence of the received voltage on the distance z from the focal position is:

$$V(z) = \int_0^{\pi/2} P(\theta)R(\theta)e^{-i2zk\cos\theta}\sin(\theta)\cos(\theta)d\theta,$$

(1)

where θ is the angle between the beam axis and the normal vector of the surface, and $k = 2\pi/\lambda$ is the wave number. $P(\theta)$ and $R(\theta)$ are the pupil function of the lens and the complex reflectance function, respectively [20]. If the sample surface is positioned at the focus, all parts of the incoming spherical wave front are in phase, and plane wave propagation can be assumed. The reflection is then proportional to the angular dependent reflectance function $R(\theta)$:

$$R(\theta) = \frac{Z_1\cos^2 2\theta_S + Z_s\sin^2 2\theta_S - Z_1}{Z_1\cos^2 2\theta_S + Z_S\sin^2 2\theta_S + Z_1},$$

(2)

$$Z_1 = \frac{\rho_1 v_1}{\cos\theta}, \quad Z_l = \frac{\rho_2 v_l}{\cos\theta_l}, \quad Z_s = \frac{\rho_2 v_s}{\cos\theta_s},$$

(3)

$$\beta = k_1\sin\theta = k_l\sin\theta_l = k_s\sin\theta_s,$$

(4)

where $Z_i = \rho_i \cdot v_i$ are the acoustic impedances (ρ is the mass density, v the sound velocity). The indices l and s correspond to longitudinal and shear waves, respectively [20]. Under the condition of normal incidence (surface of the sample is perpendicular to the beam axis), the generation of shear waves is not possible, and the reflectance function can be replaced by the reflection coefficient R:

$$R = \frac{Z_2 - Z_1}{Z_2 + Z_1}.$$

(5)

The indices 1 and 2 are for the coupling fluid and the sample, respectively.

Although there are reports of $V(z)$-measurements on highly mineralized tissues such as dentin using high frequency SAM [21], [22], this technique has never been proved to be suitable for the investigation of bone. The alternate method is the well-known C-scan, in which the reflection from the surface is measured over a rectangular scan area. A major requirement for a quantitative analysis is a well prepared, flat surface in order to avoid artifacts caused by surface inclinations. It usually is assumed that this requirement is satisfied by careful sample preparation and adjustment [16], [23]–[26]. However, there are certain limitations, if biological materials are to be investigated at very high frequencies. Mechanical preparation techniques will remove softer materials more easily than stiffer ones, which always will lead to a remaining surface roughness in heterogeneous materials with varying mechanical properties [24]. Other problems arise from imperfections in the flatness of the scan plane of the microscope and in cases in which the sample surface is not perfectly parallel to the scan plane. At very high frequencies, the dimensions of these variations become comparable to the depth of focus of the acoustic lens. Therefore, it is necessary to separate topographical influences in the image contrast from those caused by varying material properties. The Multi-layer analysis procedure (Raum *et al.* [27]–[29]) aims at finding and quantifying, for each scanned point, the reflected signal amplitude at the focus of the lens that is directly related to the material properties.

II. EXPERIMENTAL PROCEDURE

A. Experimental Setup

A scanning acoustic microscope KSI SAM 2000 (Krämer Scientific Instruments, Herborn, Germany) with a broadband lens (0.8 to 1.3 GHz) and a semi-aperture angle of 50° was used. The lens was excited by a 900 MHz burst. The burst length is approximately 20 ns. In order to provide stable measurement conditions, the samples were completely immersed in a temperature-controlled water tank. All measurements were made with distilled, degassed water at 25°C. The lateral resolution under these conditions is approximately 1 μm, and the depth of focus is 7 μm, respectively. The microscope is equipped with a heterodyne circuit for amplitude detection of the radio frequency (RF) signal. In order to gain better control over existing hardware, custom hard- and software (ELIPS, CIRAMC, Windsor, Canada, and Q-BAM, Halle, Germany) was developed. A 330 kHz A/D card (PC30F, Eagle Technology, Cape Town, South Africa) converts the demodulated, integrated video signal with a resolution of 12 bit. Several images can be averaged in order to cancel mechanical noise and to further improve the voltage sensitivity. The software provides full access to RF-circuit settings of the microscope and controls the mechanical scanner together with precise z-stage positioning. Choosing the appropriate RF-gain and input voltage range allows acqui-

TABLE I
DENSITY, LONGITUDINAL SOUND VELOCITY, AND ACOUSTIC IMPEDANCE OF THE REFERENCE SAMPLES USED FOR CALIBRATION (STANDARD ERROR IN %).

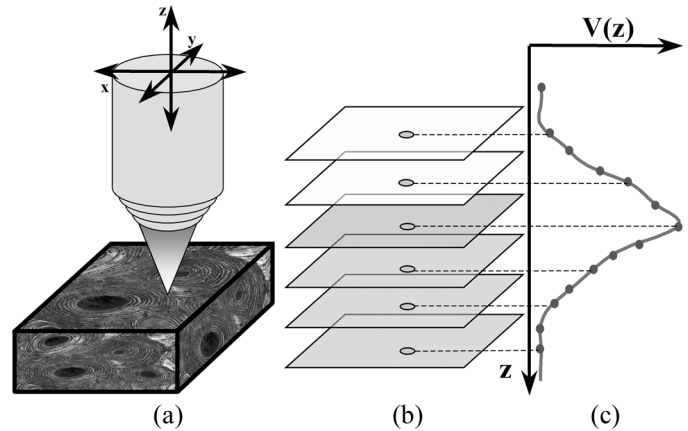| Material	Density (g/cm^3)	Longitudinal sound velocity (m/s)	Impedance (Mrayl)
Polycarbonate	1.20 (0.01)	2310 (0.37)	2.77 (0.38)
PMMA	1.18 (0.01)	2730 (0.27)	3.22 (0.28)
Suprasil®	2.21 (0.01)	6050 (0.08)	13.37 (0.09)

Fig. 1. A high frequency focused field, produced by an acoustic lens, is scanned in a plane parallel to the sample surface (a). For a MLA, a set of C-scan images with successively decreasing distances between lens and surface is acquired. The measurement starts at a z-position with obvious positive defocus and ends at a position with obvious negative defocus, respectively (b). The distance between adjacent acquisitions should be a fraction of the depth of focus of the lens. A specially developed software is used to find amplitude and position of the maximum in the $V(z)$-signal for each xy-scan position (c).

sition of images with close to linear relationship between voltage and acoustic reflectivity. Digital images with a size of up to 512 by 512 pixels are stored with a resolution of 8 bit. Scan sizes ranging from 70 μm up to approximately 1 mm squared are possible. With the ELIPS software, a set of C-scan images at successively decreasing z-positions can be measured. The image set is captured and stored automatically. Special software was developed for the data analysis using Matlab 6.1®(Mathworks Inc., Natick, MA).

B. Samples

A raster grid was used for the calibration of the spatial parameters of the system. The grids have a spacing of 10 μm and a bar width of 2 μm, respectively. The elevation of the plateaus is approximately 0.3 μm.

A variety of homogenous materials served as references for impedance calibration (polycarbonate; polymethylmethacrylate, PMMA; quartz glass, Suprasil®, Heraeus Quarzglas GmbH & Co. KG, Hanau, Germany). Speed of sound and mass density of these materials were de-
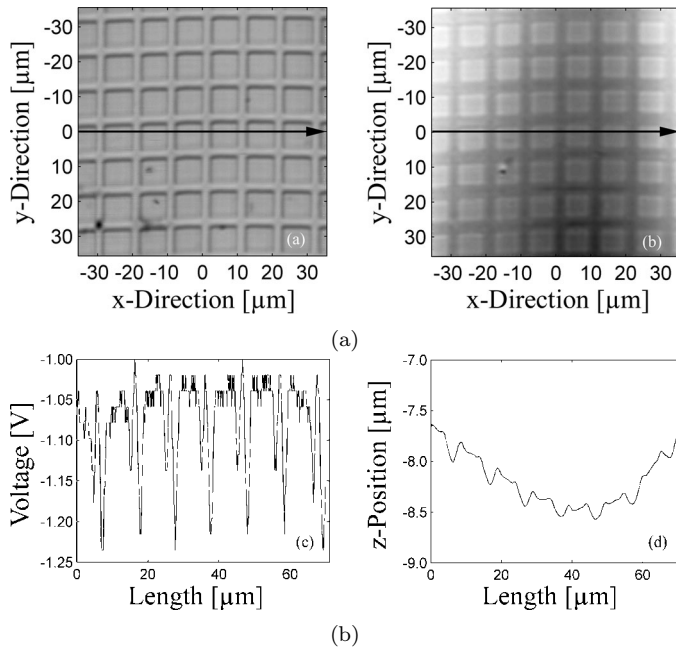
Fig. 2. Maximum image (a) and topography (b) of a raster grid plate. The values along the arrows in the images are drawn below [(c) and (d)]. The z-position in (b) and (d) is determined by the position of the maximum in the $V(z)$-curve for each xy-scan position. Locations with a significant surface inclination or edges have a decreased signal amplitude in the maximum image.
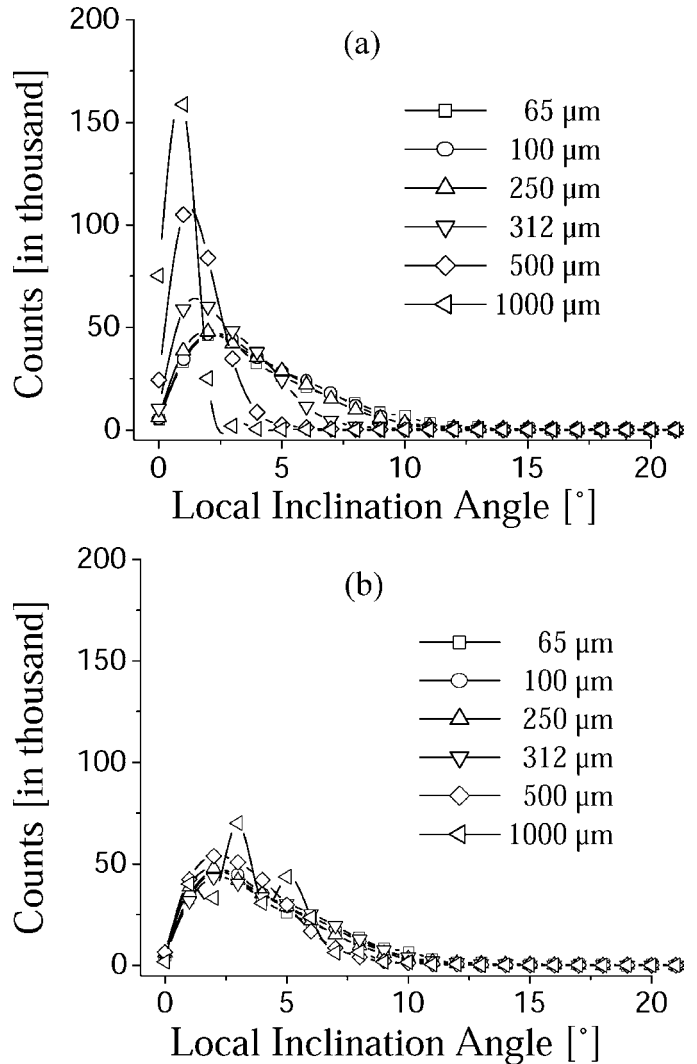

Fig. 3. Histograms of the calculated local inclination angles of the raster grid plate for different scan fields. Larger scan increments lead to an underestimation of the angle of incidence (a). A correction is possible for scan sizes up to $(500 \ \mu m)^2$ (b).

termined by a low-frequency substitution method and by Archimedes' principle, respectively (Table I).

Proximal cortical bone sections were obtained from human cadaver femora approximately 10 cm beneath the femoral head. After dehydration, the specimens were embedded in PMMA. The addition of a softener (5% dibuthylphtalate) ensured optimal conditions for the following mechanical preparation. After cutting the sample perpendicular to the femoral long axis, the surface was prepared by a grinding and polishing procedure down to a grain size of 0.25 μm.

C. Multilayer Analysis Procedure

With the proposed multilayer analysis (MLA), a set of C-scan images is acquired (Fig. 1). Starting from a z-position, in which the focus of the lens is well above the sample surface (positive defocus), images are captured with a successively decreasing lens-surface distance. The image acquisition is stopped when the focus is well below the surface everywhere in the scanned image (negative defocus). Positive as well as negative defocus conditions are characterized by significantly decreased signal amplitudes. The z-distance between two adjacent images should be a fraction of the depth of focus of the lens. In this way it is guaranteed that each scanned surface point is measured at or close to the focus once. The three dimensional data set is then resampled in z-direction using an anti-aliasing finite-impulse-response lowpass filter (built-in resample function

of the signal processing toolbox of Matlab 6.1®) in order to avoid spatial frequency components, which are larger than the initial sampling frequency in z-direction [Fig. 1(c)]. The new sampling increment can be in the order of a fraction of the acoustic wavelength.

The confocal position at each xy-scan point corresponds to the position of the maximum signal amplitude in the z-direction. Although the value of the maximum is proportional to the reflectivity, the position is a measure of the distance between an arbitrary xy-scan plane and the sample surface. These values are used to compute the two-dimensional surface topography and a topographically corrected amplitude map. The accuracy of the reconstruction of the topography is improved by applying a circular mean filter with a diameter equal to the beam width of the lens. For each point the gradients in x and y directions are determined, which allows an estimation of the local inclination angles.
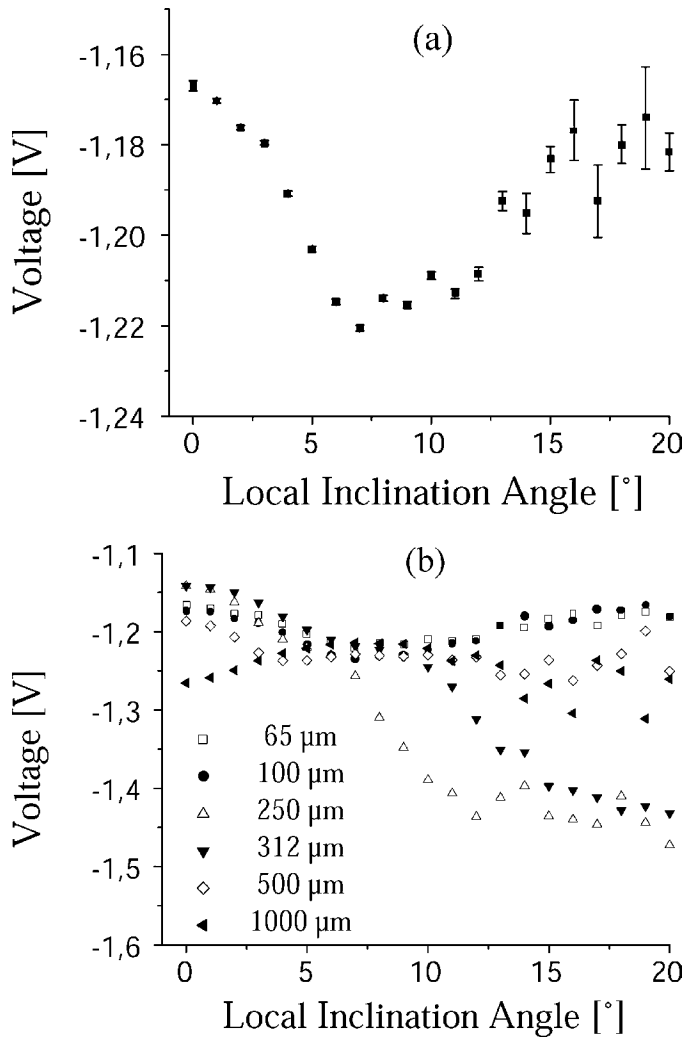
Fig. 4. Mean and standard error of the voltage values of the maximum image from Fig. 2(a) as a function of the local inclination angle (a). The voltage is negative because of a negative offset of -5 V. Up to the critical angle of total reflection, the amplitude decreases continuously (at $7°$ the amplitude is 1.35% less compared to the value at $0°$). Mode conversions cause an increase for higher angles. The values at $0°$ as well as the shapes of the signals are almost identical for all scan sizes up to the critical angle, except for the $(1000 \ \mu m)^2$ scan field (b).
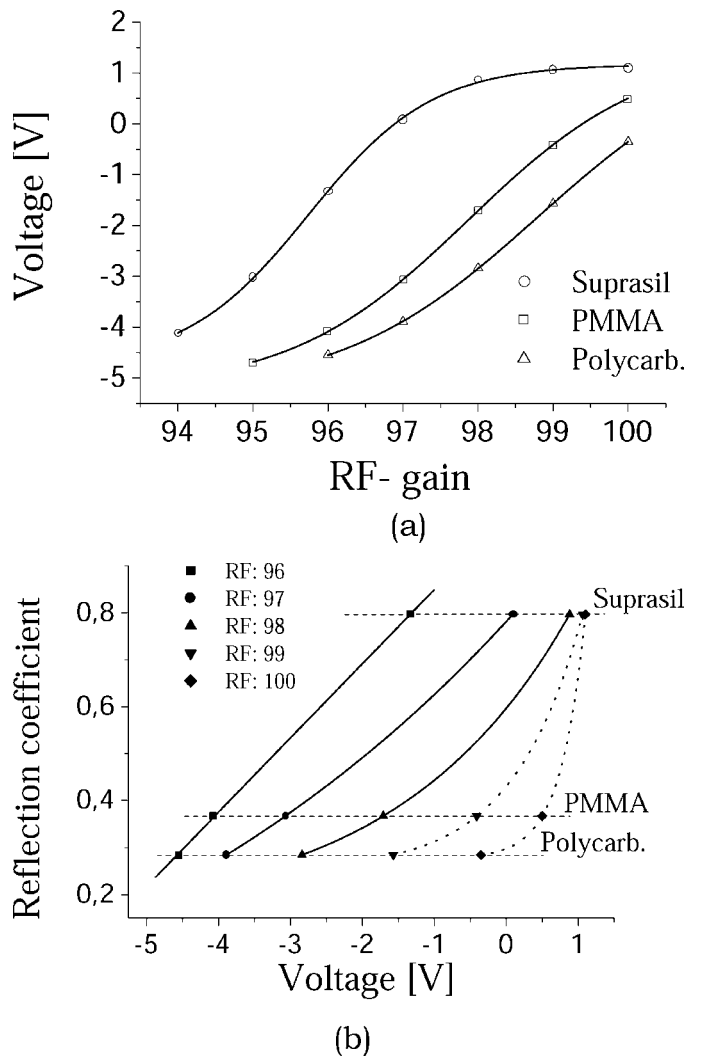
Fig. 5. Reflected amplitudes of the reference materials as a function of the RF-gain setting (a). Because of the nonlinear behavior, a reliable calibration (b) is only possible for certain gain settings (solid lines for this lens and impedance range).

III. RESULTS

A. Validation on a Raster Grid

Fig. 2 shows the reconstructed maximum map and the topography of the raster plate. The images were computed from 15 C-scan images. It can be seen in the topography that the xy-scan plane is not perfectly flat and the whole plate is slightly tilted. A system-dependent limitation is that the maximum number of pixels per scan line is 512. This causes aliasing, when larger scan fields are imaged with a high resolution lens. For the lens used here, the scan increment becomes comparable to the lateral resolution for a scan size of 500 μm by 500 μm. Therefore, this is the maximum scan field for which the topography can be reconstructed correctly.

The axial resolution of the MLA does not depend on the pulse length but on the depth of focus. The accuracy of the estimation of the focal position is of particular importance. A very high number of image acquisitions with a small increment in z-direction is not useful because the $V(z)$-signal does not contain spatial frequency components higher than the reciprocal of the depth of focus. Therefore, the resampling method mentioned above is sufficient to achieve an accuracy in the order of a fraction of the wavelength.

The values in the maximum image in Fig. 2(a) are a measure of the amplitude of the waves, which were reflected at the focus of the lens. Therefore, they are dependent only on the reflectivity of the material and on the local inclination. If the beam axis is not perpendicular to the surface, a part of the reflected wave is directed away from the transducer. However, the magnitude of the reflectance function usually decreases continuously until the critical angle for the total reflection of the longitudinal
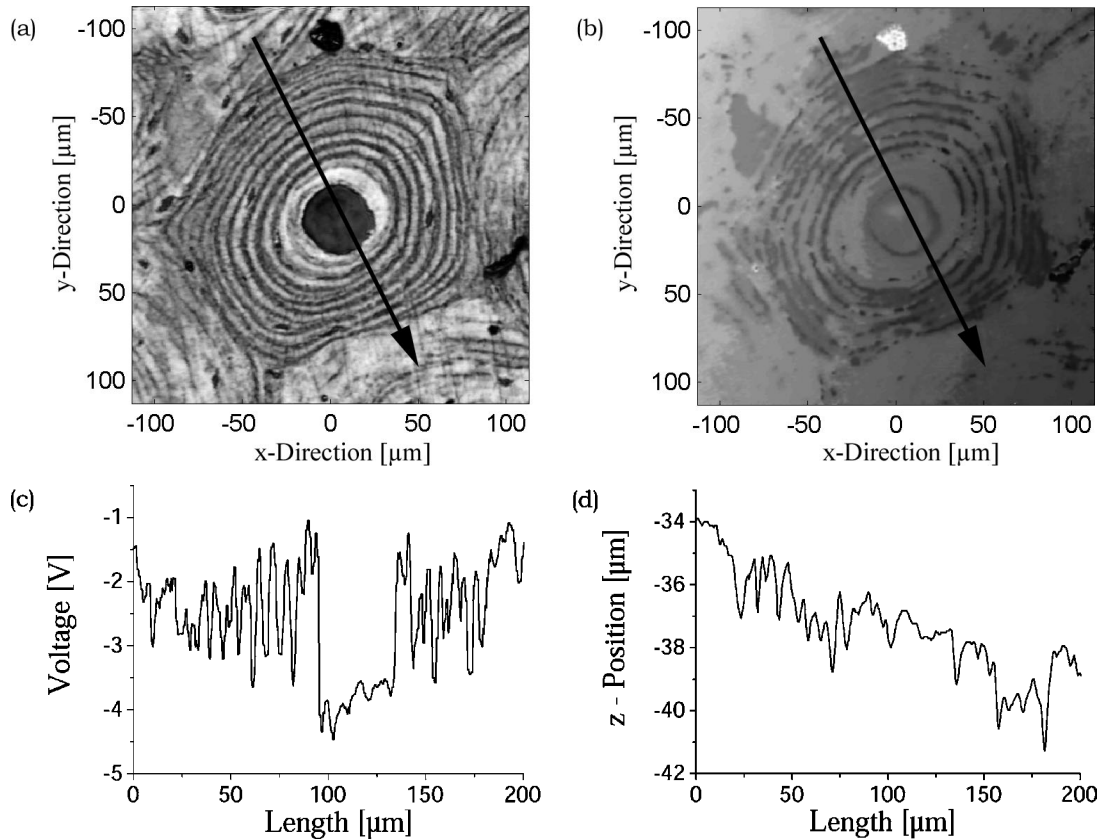
Fig. 6. Maximum and topography images of an osteon [(a) and (b)]. The Haversian channel (which is filled with the embedding material) in the center is surrounded by alternating lamellae of mineralized collagen fibers. Adjacent to the circular osteon, fractions of less structured secondary osteons are visible. The small dark spots are cavities, which used to host bone cells. The values along the plotted lines in the images are drawn in (c) and (d).

wave is reached. For angles higher than the critical angle, the reflection cannot be characterized easily anymore. Therefore, it is useful to determine the local inclination of the surface from the topography map in order to distinguish between normal and oblique incidence reflections. It is necessary to take into account the effects caused by discrete data. It can be seen in the histogram of the inclination angles that, for small scan areas the distributions are equivalent, but larger scan increments lead to an underestimation of the local inclination [Fig. 3(a)]. Except for the largest scan field, a simple correction is possible by multiplying the estimated inclination angles with scan field-dependent factors [Fig. 3(b)].

The dependence of the signal amplitude on the angle of incidence is seen in Fig. 4. Due to the high sound velocity in the raster plate, there is a continuous decrease up to an angle of 7°. The difference between minimum and maximum is 1.35%. For higher angles there is an increase again. However, because of the small amount of pixels, the standard error is increased correspondingly.

In compact bone the value of the longitudinal wave velocity usually is much less than 5000 m/s. A corresponding critical angle would be approximately 17°. For angles much smaller than this, the complex reflectance function can be approximated by the reflection coefficient. Because

the magnitude of the reflectance function at 10° is 1.63% less compared to the value at normal incidence for PMMA, a cutoff angle of 10° was chosen for an inclination exclusion map in previous works [27]–[31]. Alternatively, the slope of the angle-dependent values can be used to extrapolate the value at normal incidence.

B. Impedance Calibration

For the points with a sufficiently small angle of incidence, the measured voltage should be proportional to the reflection coefficient. The SAM image sets were acquired at various RF-gain settings for the different reference samples. Nonlinear regression was performed for the correlation between the maximum voltage values and the corresponding calculated reflection coefficients. Nonlinear regression was used in order to compensate for saturation effects, which occurred in the RF-electronics at higher amplitudes (Fig. 5). Only the gain settings with a minor nonlinearity were used for the measurements on bone.

The reproducibility of the impedance estimation was quantified by measuring a PMMA reference sample 20 times within 1 week. Calibrated RF-gain settings as well as the operating time to measurement were arbitrary. Mean and standard error of the estimated impedance were 3.26 ± 0.13 Mrayl.
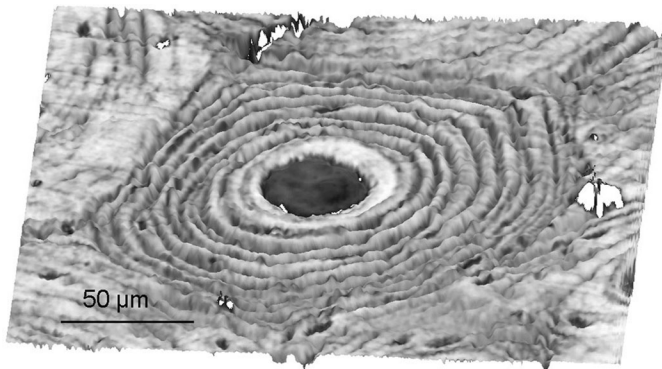
Fig. 7. Three-dimensional reconstruction of the bone surface from Fig. 6. A considerable surface roughness is visible mainly in the region of the osteon. The elevated lamellae exhibit a higher degree of reflectivity.

C. Characterization of Bone

The application of the MLA method on compact bone is illustrated in Fig. 6. The maximum and topography images were reconstructed from 17 individual C-scan images. They show a typical example of a cross section of compact bone. In the center there is an osteon with the Haversian channel (which is completely filled with the embedding material) and alternating mineralized collagen lamellae. Adjacent to the osteon parts of so-called secondary osteons are visible. Large variations of the reflectivity can be particularly seen in the osteon. It should be noted that higher values in the maximum image are well correlated with an elevation in the topography map (Fig. 7). The average distance between two elevated lamellae is approximately 8 μm, and the elevation is in the range between 1 and 2 μm. Such an increased surface roughness is not found in more homogenous regions, e.g., in the lower right secondary osteon or in the central PMMA region of the Haversian channel. The overall tilt of the sample along the arrow indicated in Fig. 6 is 1.2°.

After converting the voltages of the maximum image into values of the acoustic impedance, the mean values of certain regions of interest [Fig. 8(b)] were evaluated in three different ways. The first value was calculated regardless of the inclination angle. For the second value, the 10° exclusion map [see Fig. 8(a)] was applied prior to the calculation. Finally, the impedance was extrapolated from angular-dependent impedance plots. For the latter, the estimated value at 0° is assumed to be the impedance as defined in (5). The histograms and angular dependent plots for the three ROI's are drawn in Fig. 9. The results are summarized in Table II.

For the PMMA region, there was no difference in the mean values for methods 1 and 2 (2.90 ± 0.002 Mrayl), and the extrapolated 0° value from the angular dependent plot was slightly higher (2.93 ± 0.01 Mrayl). In the secondary osteon the mean of the histogram was 4.98 ± 0.004 Mrayl without and 5.13 ± 0.004 Mrayl with the inclination map. A considerably higher value (5.50 ± 0.05 Mrayl) was
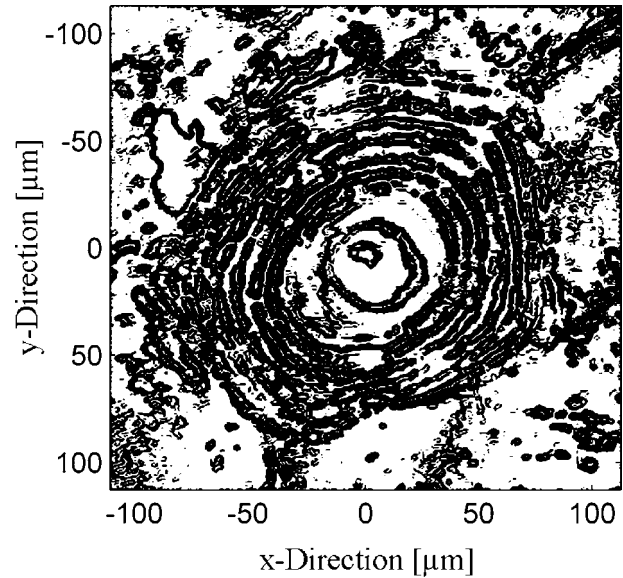

(a)
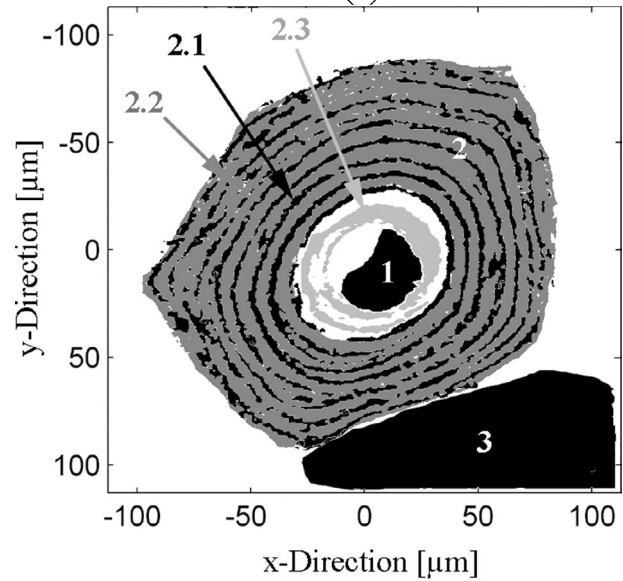
(b)

Fig. 8. A 10° inclination mask (a) and segmented regions of interests (b) of the bone surface from Fig. 6. The ROI's are: 1-PMMA, 2-osteon, 2.1-lamellae with low reflectivity, 2.2-lamellae with high reflectivity, 2.3-innermost thick lamella with very high reflectivity, 3-secondary osteon.

found with method 3. The largest differences between the calculation methods were found for the estimations of the mean impedance within the osteon. Here the values ranged from 3.94 ± 0.01 with method 1 to 5.10 ± 0.05 Mrayl with method 3.

A drawback of the angular-dependent calculation is that no impedance distributions can be calculated, mainly because of the small amount of pixels for each angle. In order to characterize individual structures, the image has to be segmented first. This was done for the osteon using thresholds. The impedances were calculated for the alternating lamellae with low and high reflectivity and for the inner-

1. - PMMA
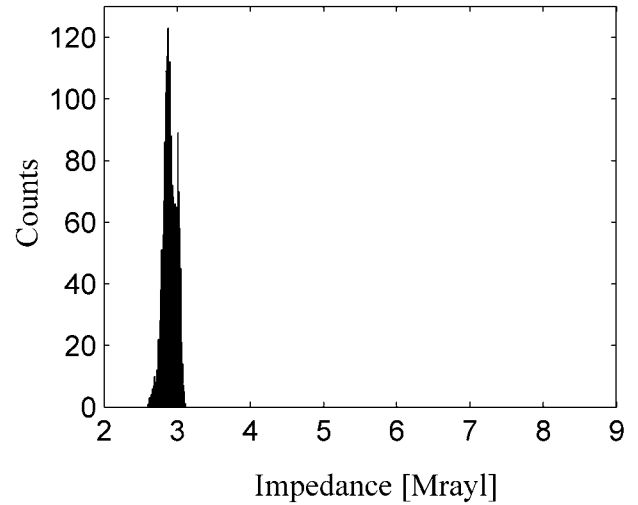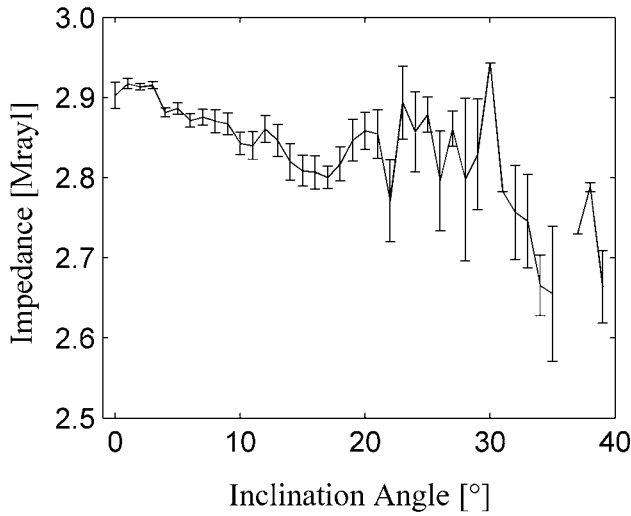
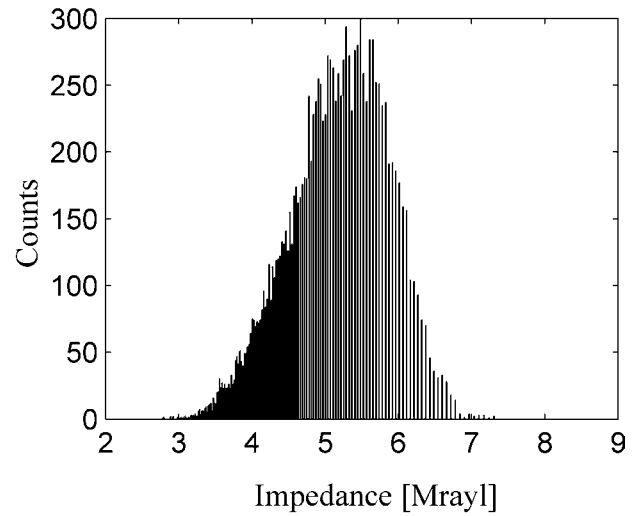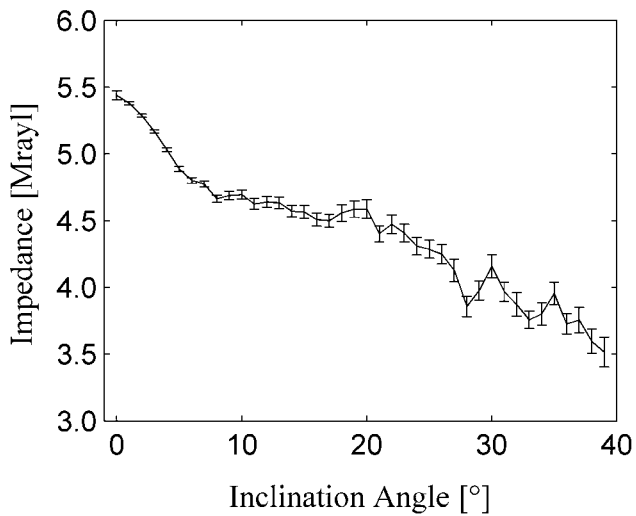2. - Osteon
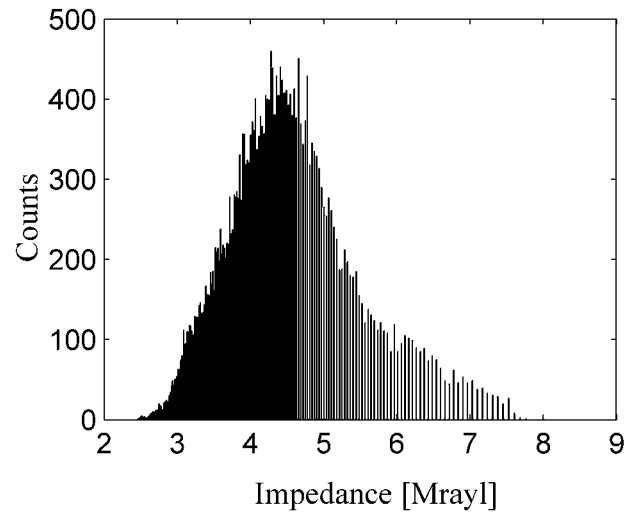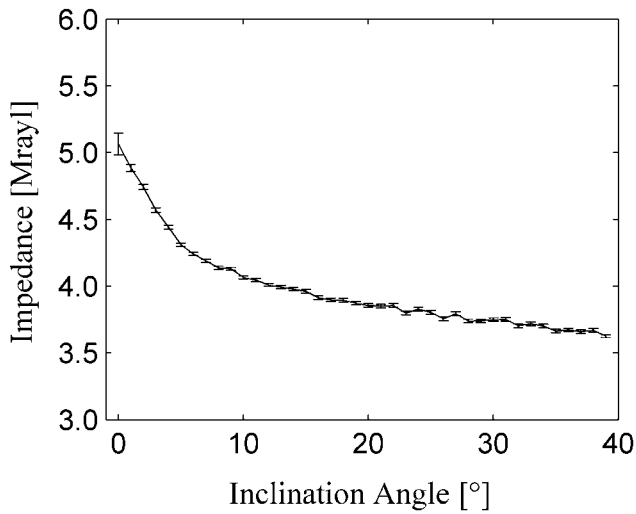
3. - Secondary Osteon

Fig. 9. Angular dependent impedance plots (left-hand side) and impedance histograms (right-hand side) of the ROI's indicated in Fig. 8(b). For the histograms, the 10° inclination map [Fig. 8(a)] was applied.

TABLE II

MEAN IMPEDANCE, STANDARD DEVIATION, AND STANDARD ERROR FOR THE ROI'S MARKED IN FIG. 8(B) (ALL VALUES IN MRAYL).

| ROI	Method 1 (all pixels)	Method 2 (all pixels with less than 10° inclination)	Method 3 (0° value from the angular plot)
1. PMMA	2.90 ± 0.10 (0.002)	2.90 ± 0.10 (0.002)	2.93 (0.01)
2. Osteon	3.94 ± 0.77 (0.001)	4.43 ± 0.91 (0.001)	5.10 (0.05)
Lamellae with low reflectivity	3.42 ± 0.34 (0.001)	3.51 ± 0.33 (0.003)	3.55 (0.03)
Lamellae with high reflectivity	4.51 ± 0.40 (0.002)	4.64 ± 0.44 (0.004)	4.68 (0.03)
Innermost lamella	5.45 ± 0.89 (0.010)	5.59 ± 0.92 (0.120)	6.40 (0.02)
3. Secondary Osteon	4.98 ± 0.79 (0.004)	5.13 ± 0.71 (0.004)	5.50 (0,05)
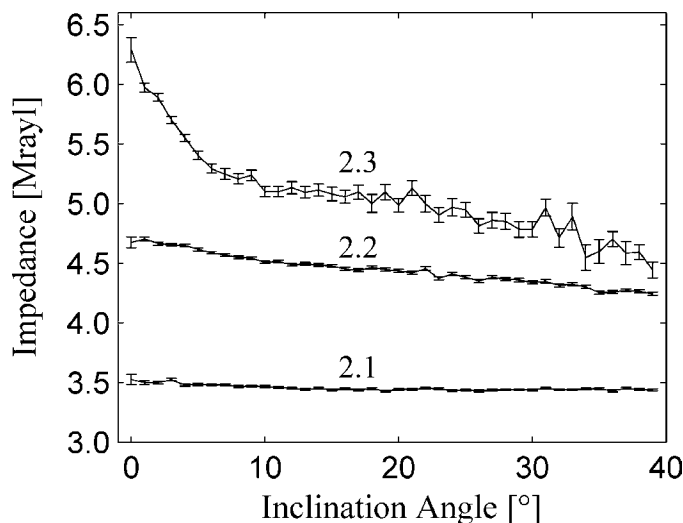
Fig. 10. Angular-dependent impedance plot of the segmented substructures of the osteon as indicated in Fig. 8(b).

most lamella, for which a significantly increased thickness and reflectivity was observed [see Fig. 8(b)]. Again, the estimation of the mean impedance from the angular plots gave the highest values (Table II). However, the angular plot of the structure with the highest impedance exhibits a much steeper slope compared to the other regions (Fig. 10).

IV. DISCUSSION

The lateral and axial resolutions of the acoustic system used here are sufficient to resolve the microstructure of cortical bone. However, after preparation a remarkable surface roughness remains, especially in highly heterogeneous regions. This general finding is in agreement with the assumption that softer materials are removed more easily during the preparation process. This in turn has considerable consequences for any quantitative evaluation. With conventional C-scan analysis, it has to be assumed that the sample surface is flat and positioned right in the focal plane. It has been shown that it is not possible to fulfill this assumption with a high frequency lens. Furthermore, neglecting the local inclination angle usually leads to significantly decreased impedance estimation in regions with a higher heterogeneity. The decrease in the measured region depends on the distribution of tilt angles as well as on the absolute impedance values. The most reliable in-

formation is obtained from angular-dependent impedance plots. The use of a 10° inclination map led to a decrease of up to 13% in regions with high impedance values; but, in regions with a low impedance, the difference was in the order of 1%. Particularly the decrease of 1% in the PMMA region is in good agreement with the estimated decrease of the reflectance function of 1.63% at 10°. The absolute value of 2.93 Mrayl is lower than the value obtained for the reference material, which is caused by the use of the softener.

For higher impedance values, the slope of the angular impedance plot is considerably steeper, which causes the higher error in the estimation. Without the consideration of the inclination angle, the error is further increased. In the osteon a maximum error of 22.7% was obtained.

It should be pointed out that the angular-impedance plots do not directly correspond to the magnitude of the complex reflectance function because the same lens is used for transmission and reception. The orientation of the local tilt is not taken into account, and the angular impedance distribution is calculated for areas rather than for a single point. Therefore, characteristic phenomena (e.g., variations of the reflectivity at the critical angle) could not be observed. However, the evaluations of the angular plots allow a more reliable estimation of the acoustic impedance for the normal incidence condition.

In a previous study by Smitmans et al. [31], in which the anisotropy, age and gender dependence of the acoustic impedance of a large number of human cortical bone samples was investigated, a significantly decreased impedance compared to low-frequency values was observed. The MLA technique in combination with the 10° inclination map was used there to estimate the impedance. With the results shown in this paper, it is hypothesized that at least a part of the decrease can be attributed to the insufficient consideration of the inclination angle.

V. CONCLUSIONS

With conventional C-scan analysis, it is neither possible to detect nor to compensate for the surface topography. However, the latter has a considerable influence on the image contrast with high-resolution SAM. A sophisticated data analysis is necessary, if composite materials are to be evaluated. The results demonstrate that the use of the MLA technique for image acquisition and data analy-

sis provides beneficial information for quantitative evaluations. With an a-priori knowledge of major system parameters, and its implementation in the data analysis, artifacts are reduced. Topographical influences on the image contrast are precisely separated from those caused by varying material properties. Image segmentation allows a reliable evaluation of the acoustical properties of biological structures at a microscopic scale. The restriction of a perfectly flat sample surface is weakened because the angular dependence of the reflectivity can be used to extrapolate the normal incidence reflection coefficient. It can be assumed that the proposed data evaluation concept will have a considerable effect on the usefulness and reliability of very high frequency SAM as a tool for quantitative micromechanical tissue characterization.

References

[1] M. L. Bouxsein and S. E. Radloff, "Quantitative ultrasound of the calcaneus reflects the mechanical properties of calcaneal trabecular bone," *J. Bone Miner. Res.*, vol. 12, pp. 839–846, May 1997.

[2] S. Chaffai, F. Peyrin, S. Nuzzo, R. Porcher, G. Berger, and P. Laugier, "Ultrasonic characterization of human cancellous bone using transmission and backscatter measurements: Relationships to density and microstructure," *Bone*, vol. 30, pp. 229–237, Jan. 2002.

[3] C. Chappard, P. Laugier, B. Fournier, C. Roux, and G. Berger, "Assessment of the relationship between broadband ultrasound attenuation and bone mineral density at the calcaneus using BUA imaging and DXA," *Osteoporos. Int.*, vol. 7, pp. 316–322, 1997.

[4] S. Cheng, F. A. Tylavsky, E. S. Orwoll, J. Y. Rho, and L. D. Carbone, "The role of collagen abnormalities in ultrasound and densitometry assessment: In vivo evidence," *Calcif. Tissue Int.*, vol. 64, pp. 470–476, 1999.

[5] S. M. Han and J. Y. Rho, "Dependence of broadband ultrasound attenuation on the elastic anisotropy of trabecular bone," *Proc. Inst. Mech. Eng.*, vol. 212, pp. 223–227, 1998.

[6] D. Hans, C. Wu, C. F. Njeh, S. Zhao, P. Augat, D. Newitt, T. Link, Y. Lu, S. Majumdar, and H. K. Genant, "Ultrasound velocity of trabecular cubes reflects mainly bone density and elasticity," *Calcif. Tissue Int.*, vol. 64, pp. 18–23, Jan. 1999.

[7] P. Laugier, P. Droin, A. M. Laval-Jeantet, and G. Berger, "In vitro assessment of the relationship between acoustic properties and bone mass density of the calcaneus by comparison of ultrasound parametric imaging and quantitative computed tomography," *Bone*, vol. 20, pp. 157–165, Feb. 1997.

[8] P. H. Nicholson, R. Muller, G. Lowet, X. G. Cheng, T. Hildebrand, P. Ruegsegger, G. van der Perre, J. Dequeker, and S. Boonen, "Do quantitative ultrasound measurements reflect structure independently of density in human vertebral cancellous bone?," *Bone*, vol. 23, pp. 425–431, Nov. 1998.

[9] K. A. Wear, "Anisotropy of ultrasonic backscatter and attenuation from human calcaneus: Implications for relative roles of absorption and scattering in determining attenuation," *J. Acoust. Soc. Amer.*, vol. 107, pp. 3474–3479, June 2000.

[10] C. M. Daft, G. A. Briggs, and W. D. O'Brien, "Frequency dependence of tissue attenuation measured by acoustic microscopy," *J. Acoust. Soc. Amer.*, vol. 85, pp. 2194–2201, May 1989.

[11] M. Tanaka, H. Okawai, N. Chubachi, R. Suganuma, and K. Honda, "Acoustic microscope for the tissue characterization in medicine and biology," in *Ultrasonic Tissue Characterization*. F. Dunn, Ed. Tokyo: Springer-Verlag, 1996, ch. 10.

[12] S. Han, J. Y. Rho, J. Medige, and I. Ziv, "Ultrasound velocity and broadband attenuation over a wide range of bone mineral density," *Osteoporos. Int.*, vol. 6, pp. 291–296, 1996.

[13] O. V. Kolosov, V. M. Levin, R. G. Maev, and T. A. Senjushkina, "The use of acoustic microscopy for biological tissue characterization," *Ultrasound Med. Biol.*, vol. 13, pp. 477–483, Aug. 1987.

[14] S. Lees and D. Z. Klopholz, "Sonic velocity and attenuation in wet compact cow femur for the frequency range 5 to 100 MHz," *Ultrasound Med. Biol.*, vol. 18, pp. 303–308, 1992.

[15] J. Y. Rho, "An ultrasonic method for measuring the elastic properties of human tibial cortical and cancellous bone," *Ultrasonics*, vol. 34, pp. 777–783, 1996.

[16] S. J. Shieh, M. C. Zimmerman, and N. A. Langrana, "The application of scanning acoustic microscopy in a bone remodeling study," *J. Biomech. Eng.*, vol. 117, pp. 286–292, Aug. 1995.

[17] M. C. Zimmerman, A. Prabhakar, B. V. Chokshi, N. Budhwani, and H. Berndt, "The acoustic properties of normal and imbedded bovine bone as measured by acoustic microscopy," *J. Biomed. Mater. Res.*, vol. 28, pp. 931–938, Aug. 1994.

[18] S. Weiner and H. D. Wagner, "The material bone: Structure mechanical function relations," *Ann. Rev. Mater. Sci.*, vol. 28, pp. 271–298, 1998.

[19] R. A. Lemons and C. F. Quate, "Acoustic microscope—scanning version," *Appl. Phys. Lett.*, vol. 24, pp. 163–165, 1974.

[20] G. A. Briggs, *Acoustic Microscopy*. Oxford: Clarendon, 1992.

[21] T. N. Gardner, J. C. Elliott, Z. Sklar, and G. A. Briggs, "Acoustic microscope study of the elastic properties of fluorapatite and hydroxyapatite, tooth enamel and bone," *J. Biomech.*, vol. 25, pp. 1265–1277, Nov. 1992.

[22] S. D. Peck, J. M. Rowe, and G. A. Briggs, "Studies on sound and carious enamel with the quantitative acoustic microscope," *J. Dent. Res.*, vol. 68, pp. 107–112, Feb. 1989.

[23] K. Hasegawa, C. H. Turner, R. R. Recker, E. Wu, and D. B. Burr, "Elastic properties of osteoporotic bone measured by scanning acoustic microscopy," *Bone*, vol. 16, pp. 85–90, Jan. 1995.

[24] J. L. Katz and A. Meunier, "Scanning acoustic microscope studies of the elastic properties of osteons and osteon lamellae," *J. Biomech. Eng.*, vol. 115, pp. 543–548, Nov. 1993.

[25] J. L. Katz and A. Meunier, "Scanning acoustic microscopy of human and canine cortical bone microstructure at high frequencies," *Stud. Health Technol. Inform.*, vol. 40, pp. 123–137, 1997.

[26] Z. L. Yu and S. Boseck, "Scanning acoustic microscopy and its applications to material characterization," *Rev. Mod. Phys.*, vol. 67, pp. 863–891, Oct. 1995.

[27] K. Raum, J. Brandt, A. Klemenz, and U. Cobet, "Quantitative scanning acoustic microscopy for the determination of the elastic properties of cortical bone," *Z. Med. Phys.*, vol. 9, pp. 246–253, 1999.

[28] K. Raum, J. Brandt, A. Klemenz, and U. Cobet, "Advanced measurement techniques for a quantitative characterization of the microstructure of bone using a scanning acoustic microscope," in *Proc. Int. Conf. Comp. Eng.*, 1999, pp. 691–692.

[29] K. Raum, U. Cobet, L. Smitmans, and J. Brandt, "Quantitative scanning acoustic microscopy of cortical bone using a multi layer analysis method," in *Proc. IEEE Ultrason. Symp.*, 1999, pp. 593–596.

[30] K. Raum, J. Brandt, A. Klemenz, and U. Cobet, "Quantitative Akustische Rastermikroskopie zur Bestimmung der elastischen Eigenschaften von kortikalem Knochengewebe," in *Tagungsband Medizinische Physik*, 1998, pp. 199–200. (in German)

[31] L. Smitmans, K. Raum, J. Brandt, and A. Klemenz, "Variations in the microstructural acousto-mechanical properties of cortical bone revealed by a quantitative acoustic microscopy study," in *Proc. IEEE Ultrason. Symp.*, 2001, pp. 1379–1382.

Kay Raum (M'02) was born in Halle, Germany, on March 1, 1972. He received the diploma and Ph.D. degrees in physics from the Martin Luther University of Halle in 1997 and 2002, respectively.

From 1995–1996 he was with the Bioacoustics Research Laboratory at the University of Illinois at Urbana-Champaign as a visiting scholar. From 1997 until 2002 he was with the Institute of Medical Physics and Biophysics at Martin Luther University. Now he has joined the Department of Orthopedics of the Medical Faculty of the Martin Luther University.

His areas of interest are high frequency acoustic imaging and signal processing for the quantitative evaluation of biological tissues.

Klaus V. Jenderka (M'96) was born in Oschatz, Germany, on May 8, 1961. He received his diploma in physics in 1985 and his Ph.D. in physics in 1990, both from the Martin Luther University, Halle-Wittenberg, Germany.

During 1988–1992 he was a research assistant at the Martin Luther University. From 1992 to 1994 he was involved in a research project dealing with tissue ischemia at the University of Goettingen, Germany. Since 1995 he has been a research assistant at the Martin Luther University, Institute of Medical Physics and Biophysics. His main fields of interests are ultrasound imaging and tissue characterization.

Dr. Jenderka is a member of the German Society of Ultrasound in Medicine (DEGUM).

Jörg Brandt was born in Leipzig, Germany, on August 8, 1962. He received his diploma in medicine in 1985 and his Ph.D. in medicine in 1988, both from the University of Leipzig, Germany.

From 1990 to 1996 he was a medical assistant at the Leipzig University hospital until finishing his specialization in orthopedics in 1996. In 1993 he worked in a research project on bone-implant-interfaces at the Technical University of Munich. Since 1996 he is the scientific head of the research laboratory of the Department of Orthopedics of the Martin Luther University of Halle-Wittenberg, Germany. His research is mainly focused on orthopedic implants, bone-implant-interfaces, acoustic microscopy and the biology of bone and cartilage cells.

Albrecht Klemenz was born in Leipzig, Germany, on December 21, 1952. He received his diploma in physics in 1976 and his Ph.D. in physics in 1987, both from the Martin Luther University, Halle-Wittenberg, Germany.

Since 1978, he has been a research assistant at the Martin Luther University, Medical Department, Institute of Medical Physics and Biophysics. His research interests include ultrasound microscopy and ultrasound scattering. Dr. Klemenz is a member of the German Society of Medical Physics (DGMP) and the German Society of Ultrasound in Medicine (DEGUM).